Measurements and a direct-reaction–plus–Hauser-Feshbach analysis of $^{89}Y(p,n)^{89}Zr$, $^{89}Y(p,2n)^{88}Zr$, and $^{89}Y(p,pn)^{88}Y$ reactions up to 40 MeV

M. G. Mustafa, H. I. West, Jr., H. O'Brien,* R. G. Lanier, M. Benhamou,† and T. Tamura‡
Nuclear Chemistry Division, Lawrence Livermore National Laboratory, University of California, Livermore, California 94550
(Received 4 April 1988)

We report measurements and analyses of cross sections up to 40 MeV for the reactions $^{89}Y(p,n)^{89}Zr$, $^{89}Y(p,2n)^{88}Zr$, and $^{89}Y(p,pn)^{88}Y$ obtained by the foil-activation method. The data are compared with other measurements and analyzed by the Hauser-Feshbach plus one- and two-step direct reactions. The analysis shows that Hauser-Feshbach plus one-step direct reaction is adequate to explain the data. The cross sections are also calculated with phenomenological preequilibrium models (exciton, hybrid, and geometry-dependent hybrid models), using global parameters. However, to get a good fit to the data with these phenomenological models, some adjustments of the global parameters were necessary. A discussion on the differences between the direct-reaction theory and preequilibrium models is given.

I. INTRODUCTION

Measuring reaction cross sections via induced radioactivity is a classic subject in nuclear physics. The reaction cross sections are extracted not by observing emitted particles, but by measuring beta-decay gamma rays characteristic of the nuclei that result from various reactions. The experiments thus measure the total production cross sections of various nuclei. This paper deals with the measurements and analysis of some reactions induced by protons upon ^{89}Y. In Sec. II we briefly discuss our experimental method and compare our data with other measurements.

Excitation functions are usually analyzed quite successfully by assuming that a compound nucleus is formed first, followed by the evaporation of some number of nucleons from it. Here we use protons with bombarding energies as high as 40 MeV, and in this high-energy region, the classical evaporation analysis becomes insufficient. Thus the combined use of direct- and compound-reaction analyses becomes unavoidable.

In a recent pair of papers,[1,2] we discussed $^{52}Cr(d,2n)^{52}Mn^{g,m}$ reactions. Since the cross sections were measured via activity, the experimental data available were simply two excitation functions for the formation of $^{52}Mn^{g}$ and $^{52}Mn^{m}$. However, to fit these excitation functions, both of which were rather smooth, we had to apply techniques that are being used currently in the analyses of various direct reactions. Specifically, we had to assume that only the inner part of the imaginary potential is responsible for the formation of the compound nucleus, a concept very successfully applied to the analysis of heavy-ion fusion data.[3] We also had to apply the idea of the "breakup-fusion" reaction,[4] which is currently one of the most exciting subjects in the study of nuclear reactions. Our work in Ref. 2 thus showed that the rather simple looking excitation function data of Ref. 1 contained a large amount of intriguing physical information.

The analysis of the proton-induced reaction was not as involved as was the deuteron-induced reaction.[2] We were able to fit the data simply as a sum of Hauser-Feshbach (HF)[5] and continuum direct-reaction cross sections.[6,7] We discuss these results in Sec. III. Furthermore, since such data were extensively analyzed in the past using semiclassical preequilibrium models (exciton, hybrid, and geometry-dependent hybrid), we show some results calculated with these models in Sec. IV. The results of the preequilibrium models are reconciled with the direct-reaction results in Sec. V, followed by a summary in Sec. VI.

II. EXPERIMENTAL RESULTS

A. Experimental method

We used the foil-activation method to obtain the excitation functions. In this method, a stack of yttrium foils, interspersed with aluminum foils, is irradiated with an accurately measured beam of particles. The induced activities (in this case gamma rays) are counted off line; then, from an accurate knowledge of the nuclear decay scheme, a cross section is calculated. Properly used, the method is capable of considerable accuracy. This method is discussed in detail in our paper on the $^{52}Cr(p,n)^{52}Mn^{g,m}$ and $^{52}Cr(d,2n)^{52}Mn^{g,m}$ excitation functions.[1] Here we give only the essentials.

We performed our experiments at the Lawrence Livermore National Laboratory (LLNL)'s Cyclograaff for 0- to 20-MeV protons and used the cyclotron at the Crocker Nuclear Laboratory (CNL) of the University of California at Davis to extend the measurements to 40 MeV.

The irradiation chamber (see Ref. 1) functioned as a Faraday cup. The beam current was measured by an ORTEC model 439 digital current integrator. The unit has a precision of 0.01% and an absolute accuracy of 0.2%. Typical beam currents were 1 μA, with a total collected charge of 1000 μC.

Our targets were of a purity 99.5 and 99.9% and were obtained from two independent vendors. Densities varied from 5 to 11 mg/cm^2 and the foils were 25.4 mm in diameter. (Most of the beam was intercepted by the central 8-mm-diam region.) Catcher foils of aluminum, typically 0.0254 mm thick, were used to catch ions recoiling out the back of the primary foils. A count of their activity relative to that of the primary foil gave information on the momentum transfer during the reaction. Additional aluminum foils were used as energy degraders. A typical foil stack consisted of one to five yttrium foils, the number depending upon how rapidly the cross section varied with energy in the region of interest. From fluorescent x-ray studies on typical foils, we estimate that any uncertainties in the cross sections due to density gradients in the yttrium foils were less than ±2%. In those few cases where we found the density variation to be several percent, corrections to the data were necessary.

Gamma counting was done using the Nuclear Chemistry Division's automated germanium counters. The data were analyzed using the code GAMANAL.[8] Uncertainties due to absolute calibration error in the counting system may be as large as ±2%. Intercomparison between counters and comparison with standards would seem to indicate that this is a safe limit on the uncertainty. Figure 1 shows the essentials of the decay scheme used for ^{89}Zr decay. These results are from Lederer *et al.*[9] except for the half-life of ^{89}Zr (Ref. 10). Note the decay from the isomeric level, which reduces the ground-state population of ^{89}Zr by several percent. The essentials of the ^{88}Zr-^{88}Y-^{88}Sr decay that we used are shown in Fig. 2. The half-life of the ^{88}Zr decay is from Bayhurst and Butler.[11] From our measurements of gamma-ray intensity ratio $I(898)/I(1836)=0.9441$, and using the other values (weak γ branches, conversion coefficients, and β^+ intensity) from Lederer *et al.*,[9] we have assigned slightly different values of the branchings to the two low-lying states in ^{88}Sr than those given in Lederer *et al.* The I_γ we used for each transition is indicated which resulted in cross sections ~1% lower than that from using the old values. For the ^{88}Y decay, both the 898- and 1836-keV gamma-ray counts were used. For these two gamma rays, coincidence summing could cause loss in the photo peaks in the germanium spectrum. Corrections as large as 1% were made for this effect. To prevent loss due to coincidence summing with x-rays and to define the region of β^+ annihilation, we routinely used 1.275-g/cm^2 aluminum absorbers in our counting.

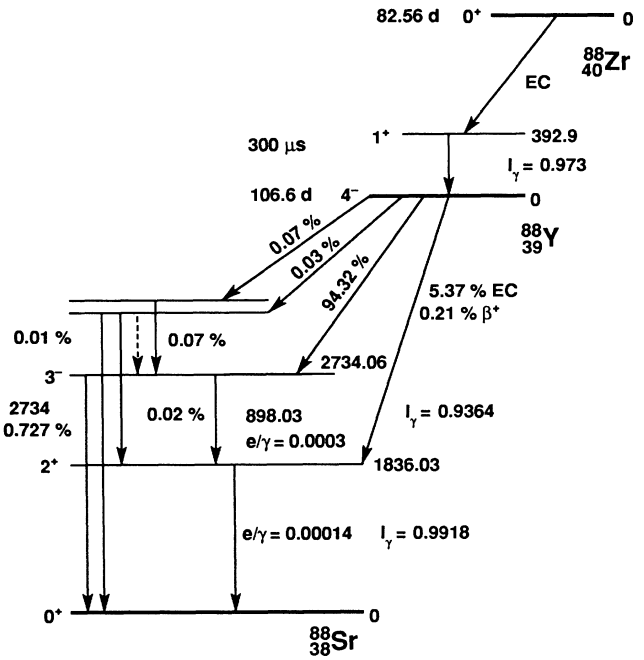

FIG. 2. Essentials of the ^{88}Zr-^{88}Y-^{88}Sr decay scheme.

The dominant errors are thus ±2% for foil uniformity and ±2% for counter calibration. Decay-scheme errors are insignificant in comparison. The data are reported in Table I. The errors assigned there are primarily statistical. To these errors, the error for foil uniformity and counter calibration should be added in quadrature.

B. The data

We show the results in Table I. These measurements are the result of different runs taken over the period of a year. Most of the data below 21 MeV were acquired using the LLNL Cyclograaff, with a few points at 10 to 18 MeV coming from the Los Alamos National Laboratory (LANL) Van de Graaff. The energies for the Cyclograaff and Van de Graaff were known to at least ±20 keV. Above 20 MeV we used data from the CNL cyclotron. The region of overlap is indicated in Table I. The energies were determined by the operators using the gamma-flash method and were known to ±100 keV. In each case, the initial beam spread was about the same as the energy uncertainty. Straggling, however, increased the beam spread considerably. The quantity ΔE in column two is the total beam spread in the foil, which consists of energy loss convoluted with the straggling.

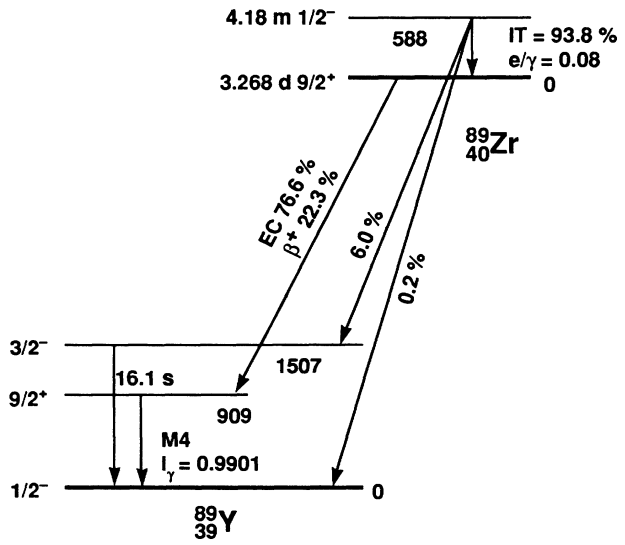

FIG. 1. Essentials of the ^{89}Zr-^{89}Y decay scheme.

TABLE I. Excitation functions for the $^{89}Y(p,n)^{89}Zr$, $^{89}Y(p,2n)^{88}Zr$, and $^{89}Y(p,pn)^{88}Y$ reactions.

E_p^{lab} (MeV)	ΔE (MeV)[a]	^{89}Zr[b] σ (mb)	^{88}Zr σ (mb)	^{88}Y σ (mb)
4.59	0.23	17.15±0.05[c]		
4.78	0.44	26.3±0.1		
5.30	0.41	51.2±0.2		
5.51	0.19	70.5±0.2		
5.81	0.38	98.2±0.2		
6.31	0.19	142.4±0.3		
6.62	0.49	200.4±1.4		
6.83	0.35	224.3±0.5		
7.36	0.29	330.2±0.6		
7.90	0.37	391.1±0.9		
8.38	0.38	467.1±1.8		
8.98	0.32	520.7±1.2		
9.18	0.29	572.5±2.2		
9.88	0.41	616.6±8.0		
9.94	0.33	636.0±2.4		
10.87	0.26	674.5±1.8		
10.88	0.25	674.4±1.6		
11.97	0.17	741.5±4.7		$(2.5\pm2.6)\times10^{-3}$
12.46	0.33	750.8±1.5		
12.70	0.14	749.0±2.0		0.0123±0.0030[c]
13.30	0.11	756.2±2.1	3.62±0.09[c]	0.096±0.016
13.40	0.11	769.0±2.5	6.49±0.11	0.151±0.038
13.80	0.10	787.3±2.6	34.88±0.26	0.272±0.108
14.19	0.10	764.9±2.6	69.98±0.48	1.21±0.13
14.68	0.26	700.0±1.4	125.2±0.5	5.31±0.52
14.95	0.18	666.4±2.2	165.9±0.9	8.39±0.21
15.41	0.37	599.2±7.3	229.6±2.4	17.87±0.21
15.95	0.18	536.0±1.7	324.8±1.5	31.20±0.30
16.57	0.30	475.4±0.9	418.0±2.3	45.2±0.4
17.39	0.32	320.8±2.3	533.9±1.6	64.8±0.3
18.31	0.24	241.9±0.3	643.9±10.7	85.9±1.5
19.21	0.26	169.2±1.6	711.1±4.0	115.2±0.8

The $\sigma(E)$ for the $^{88}Y(p,n)^{89}Zr$ excitation function varies rapidly enough with energy in the rising portion of the excitation function that resolution corrections seemed to be needed, although in the final analysis this correction was but a few percent.

To obtain the corrected value of σ, we used a procedure that depends on knowing only the relative variation of the cross section with energy, which we obtain from a polynomial fit to the uncorrected data. Experimentally, we obtain an average of σ over the foil thickness Δx. We call the experimental value σ_{exp} and the corresponding calculated value σ_{av}. By definition,

$$\sigma_{av}=\frac{1}{\Delta x}\int \sigma(x)dx \ ,$$

which is an integral equation to be solved for $\sigma(x)$ under the assumption of a smoothly varying cross section. For this equation we can write

$$\sigma_{av}=\frac{1}{\Delta E}\int \frac{\sigma(E)dE}{(dE/dx)/(dE/dx)_{av}} \ .$$

Note that the term in the denominator inside the integral corrects for the fact that as dE/dx increases, less of the foil thickness is subject to irradiation for a given energy. The correction for the dE/dx variation over the foil

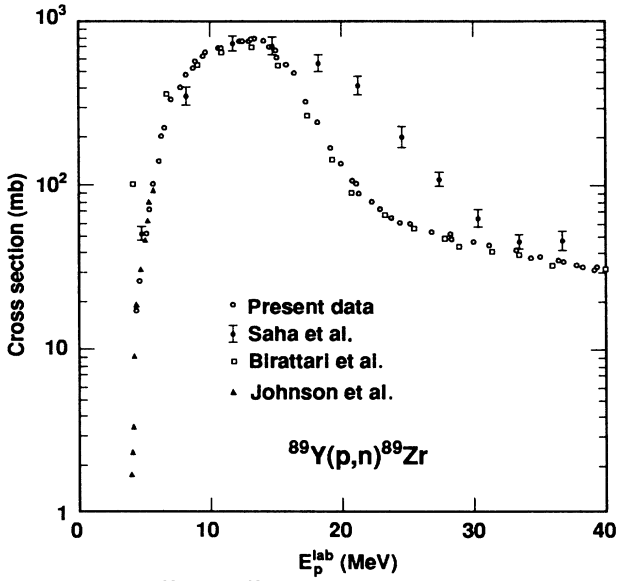

FIG. 3. The $^{89}Y(p,n)^{89}Zr$ excitation function compared with other data. The Saha *et al.* (Ref. 12) data are in great disagreement with the present data. The Birattari *et al.* (Ref. 13) data agree fairly well except for the threshold region. The data of Johnson *et al.* (Ref. 15) near threshold fit our data well within experimental error.

TABLE I (*Continued*).

E_p^{lab} (MeV)	ΔE (MeV)[a]	^{89}Zr[b] σ (mb)	^{88}Zr σ (mb)	^{88}Y σ (mb)
19.89[d]	0.44	135.3±0.2	725.8±1.4	128.4±0.4
19.92	0.17	140.8±0.5	765.0±7.4	129.8±2.1
20.87[d]	0.31	106.2±0.1	746.5±5.0	146.4±0.8
20.91	0.19	102.0±0.4	774.7±2.4	156.6±0.7
21.44[d]	0.11	89.4±0.1	765.4±1.4	163.9±0.4
22.38[d]	0.26	78.2±0.1	784.0±4.0	184.1±0.4
22.98	0.37	69.7±0.1	786.9±1.5	200.0±0.5
23.85	0.21	62.5±0.1	770.0±5.0	212.2±0.6
24.44	0.13	58.2±0.1	771.2±1.1	226.1±1.1
25.25	0.33	57.0±0.1	766.0±2.0	234.1±1.3
26.86	0.27	50.4±0.1	736.3±1.6	263.1±0.5
28.30	0.51	47.7±1.0	629.3±6.0	298.0±5.7
28.37	0.20	46.6±0.1	669.0±1.1	283.3±0.6
30.10	0.48	44.5±1.0	469.4±6.0	286.1±4.0
31.21	0.34	41.8±0.1	439.2±3.0	282.3±2.0
31.82	0.41	41.3±1.0	336.3±6.0	264.9±4.0
32.86	0.28	37.5±0.1	291.0±0.7	242.8±2.5
33.46	0.38	38.5±1.0	247.4±6.0	249.8±4.0
34.44	0.20	35.3±0.1	220.6±0.9	231.8±1.8
35.04	0.22	35.9±1.0	190.7±4.0	237.1±3.2
36.47	0.43	33.4±0.1	153.8±0.3	212.5±2.7
36.72	0.34	33.5±0.1	155.3±0.5	218.7±0.6
37.93	0.38	31.5±0.1	129.1±0.3	208.8±2.8
38.17	0.28	30.6±0.1	125.6±0.4	206.7±1.0
39.35	0.24	29.6±0.1	113.5±0.3	202.6±2.7
39.56	0.19	30.2±0.1	114.8±0.5	198.7±0.6

[a]Here ΔE is the energy loss of the incident proton corrected for straggling. The FWHM is reported. Note that, where important, corrections to $\sigma(E)$ have been made depending upon ΔE.

[b]This is the apparent cross section for the production of ^{89}Zr. No corrections have been made for the loss from the 4.18-m isomeric state to ^{89}Y prior to the start of measuring the decay of the ground state. See text for the corrections.

[c]The errors in each case represent the statistical and systematic errors. To these numbers, 2% for foil uniformity and 2% for detector calibration should be added in quadrature.

[d]Shows the region of overlap between Van de Graaff and cyclotron data, d referring to cyclotron data. Above 21.44 MeV, only cyclotron data are shown.

thickness has a minor effect except for the thickest foils, e.g., $\Delta E \sim 1$ MeV, which was not the case here. We fit the data in the rising portion of the excitation function to a polynomial in $\ln E$ [$\ln\sigma = a + b \ln E + c(\ln E)^2 \cdots$]. For each data point, we calculated σ_{av} and $\sigma(E_{av})$ from the polynomial. Corrected experimental values were obtained from $\sigma_{exp} \times \sigma(E_{av})/\sigma_{av}$. These values are given in the first five entries in Table I and are to be associated with E_{av}. The results are quite insensitive to the details of the fitting. Whether we used three points and a three-term polynomial in the least-squares fit or ten points and a five-term polynomial (piece-wise continuous), the results are about the same.

The $^{89}Y(p,n)^{89}Zr$ data of Table I are plotted in Fig. 3. Along with these results we show the results of Saha *et al.*[12] and of Birattari *et al.*[13] Saha *et al.* acquired their data by using the internal beams of the McGill University cyclotron and copper monitors. Obviously, the techniques they employed were difficult to apply, and we believe that the uncertainties for both these and their ^{88}Zr and ^{88}Y excitation function data are considerably outside the quoted error. For Birattari *et al.*, we took data from a photographic enlargement of their published data. Their results compare favorably with ours near the peak of the excitation function and at higher energies. However, there seems to be some discrepancy in the rising portion of the excitation function which could be attributed to the difficulties inherent in using cyclotrons.

From the decay scheme in Fig. 1, we note that after irradiation, both the isomeric state ($\frac{1}{2}^-$) and ground ($\frac{9}{2}^+$) are populated. Let σ_{ga} be the measured apparent cross section given in Table I. Then the true ground-state cross section σ_g is

$$\sigma_g = \sigma_{ga} - f\frac{\lambda_m}{\lambda_m - \lambda_g}\sigma_m ,$$

where f is the fraction that feeds from (m) to (g), and λ_m and λ_g are the respective decay constants. Now

$\lambda_m \gg \lambda_g$, and writing in terms of the isomer ratio we have

$$\sigma_g = \frac{\sigma_{ga}}{1+f\sigma_m/\sigma_g} = \frac{\sigma_{ga}}{1+0.938\sigma_m/\sigma_g} ,$$

and for the total cross section

$$\sigma_T = \sigma_g + \sigma_m = [\sigma_{ga}/(1+0.938\sigma_m/\sigma_g)](1+\sigma_m/\sigma_g) .$$

Gritsyna *et al.*[14] have obtained measurements of σ_m/σ_g which, along with one point from the work of Johnson *et al.*,[15] are plotted in Fig. 4. From 5 to 10 MeV, one multiplies σ_{ga} by 1.039, and from 15 to 20 MeV by 1.018.

In Fig. 5 we compare our low-energy data to data obtained by other workers. The data of Blaser *et al.*[16] are in reasonable agreement, but the lowest energy points reflect the difficulties in using cyclotrons and calculating the energy losses in the various absorbers employed. The data of Johnson *et al.* were acquired using a Van de Graaff and by counting the neutron emission. To compare this data with our data above the isomer threshold (4.244 MeV), we multiplied our data by 1.039. This correction is close to the limit of accuracy in reading the data from their graph—data which they quote to be within ±4%. (Structure in the cross section due to level excitation has been smoothed over.) It is gratifying to see results from two rather diverse procedures in such good agreement.

The ^{88}Zr data was analyzed from a simple exponential decay. However, for ^{88}Y we had to make allowance for considerable ingrowth from ^{88}Zr. The equation used was

$$N_{20} = \frac{A_2}{\lambda_2} e^{\lambda_2 t} - \frac{N_{10}\lambda_1}{\lambda_2-\lambda_1} e^{-\lambda_1 t}(e^{\lambda_2 t} - e^{\lambda_1 t}) ,$$

in which subscripts 1 refer to ^{88}Zr and 2 to ^{88}Y. N_{10} and N_{20} are the atoms at zero time, A_2 the activity at time t, and λ_1 and λ_2 are the respective decay constants. N_{10} was determined from the total ^{88}Zr counts first, before the N_{20} values were determined; this procedure makes it easier to keep track of the counting errors. (The best alternative is to solve two coupled linear equations by least squares.) Data from at least eight counts of the radiation from each foil were used to determine a cross section.

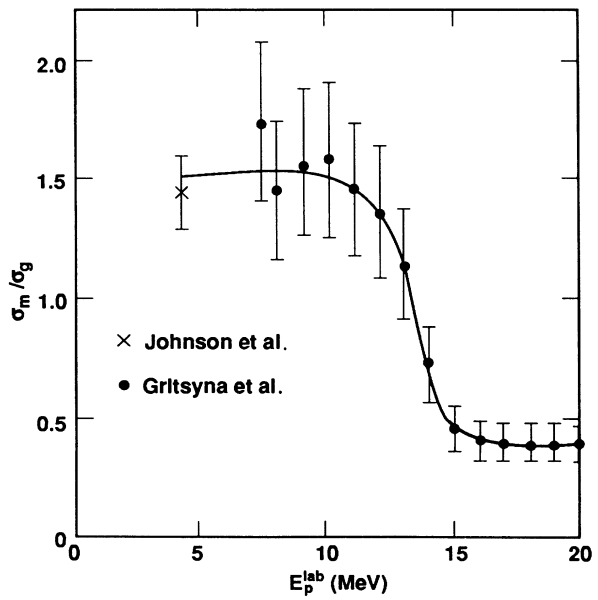

FIG. 4. Isotopic ratio σ_m/σ_g in the ^{89}Y$(p,n)^{89}$Zr excitation function. The data come from the work of Gritsyna *et al.* (Ref. 14) and Johnson *et al.* (Ref. 15).

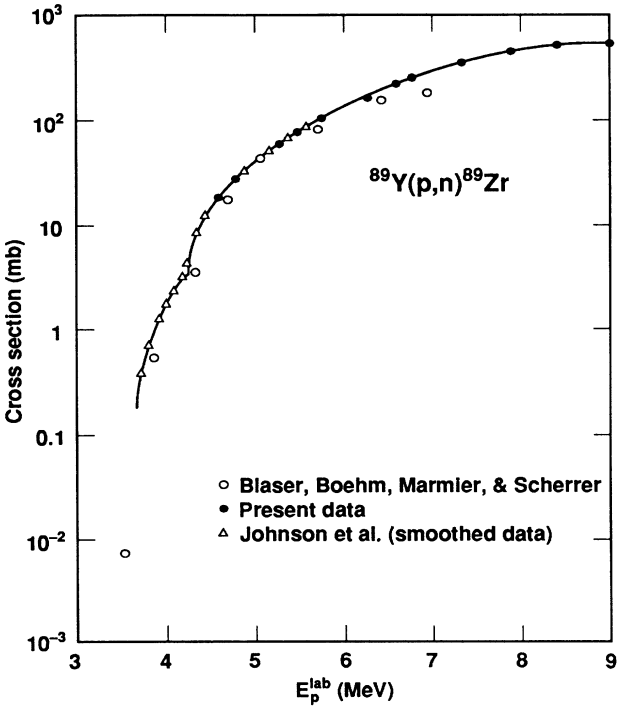

FIG. 5. Low-energy data for the ^{89}Y$(p,n)^{89}$Zr excitation function. The data of Johnson *et al.* (Ref. 15) obtained with a Van de Graaff and by counting neutrons is in quite good agreement with our data. The two resonances they observed at 4.8 and 5.0 MeV are not shown. Note that our data are increased by 4% to correct for the decay from the metastable state. The cyclotron data of Blaser *et al.* (Ref. 16) do not agree quite as well.

The ^{89}Y$(p,2n)^{88}$Zr data are tabulated in Table I (column 4) and plotted in Fig. 6. Data reported by Saha *et al.*[12] are shown also. The agreement is not very good. Saha *et al.* mention unpublished data of Gusakow[17] which were lower than their data by a factor of 1.5 to 2.0. These latter data may be better agreement at higher energies with our data than the Saha *et al.* results but are not available for evaluation.

The ^{89}Y$(p,pn)^{88}$Y data are also tabulated in Table I (column 5) and are plotted in Fig. 7. Data of Saha *et al.* are shown for comparison. Again the agreement is not good. We noted that the cross section falls rapidly well before threshold (11.609 MeV) and studied this region in some detail. The results are shown in Fig. 8. The study was hampered by the presence of the ^{88}Zr decay above its threshold at 13.076 MeV; however, we obtained two points below that point. The targets used in this region were ~6 mg/cm^2, were irradiated with ~3000 μC of

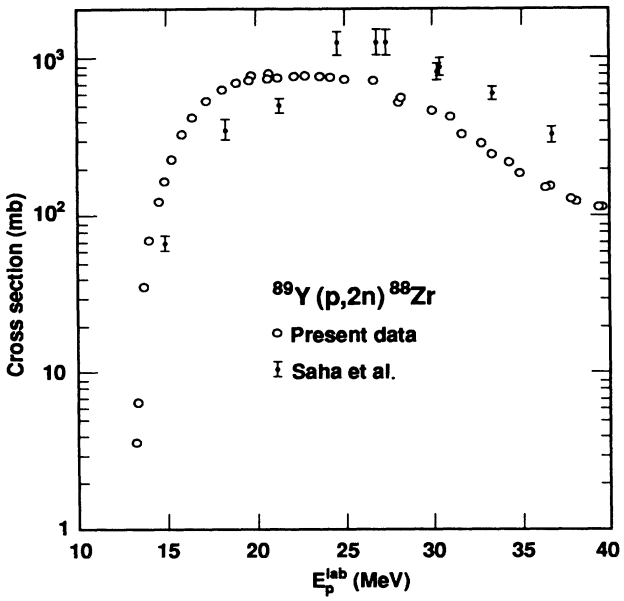

FIG. 6. The ^{89}Y$(p,2n)^{88}$Zr excitation function. Data of Saha *et al.* (Ref. 12) are shown for comparison.

protons, and were counted for one to two weeks for each data point. Interestingly, there is no evidence within our limits of measurements for the ^{89}Y$(p,d)^{88}$Y reaction with threshold at 9.36 MeV.

III. THEORETICAL ANALYSIS

A. Hauser-Feshbach (HF) calculations

The cross sections were calculated using the current Livermore version of the STAPRE code[18] of Uhl and Ströhmaier.[19] The code was designed to calculate

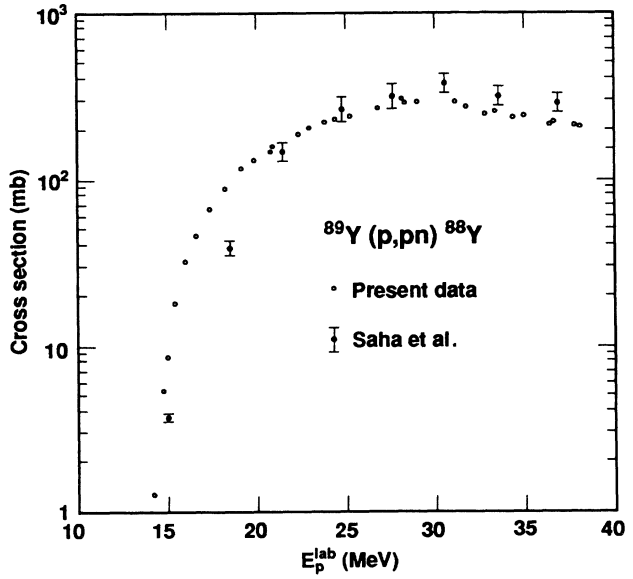

FIG. 7. The ^{89}Y$(p,pn)^{88}$Y excitation function. Data of Saha *et al.* (Ref. 12) are shown for comparison.

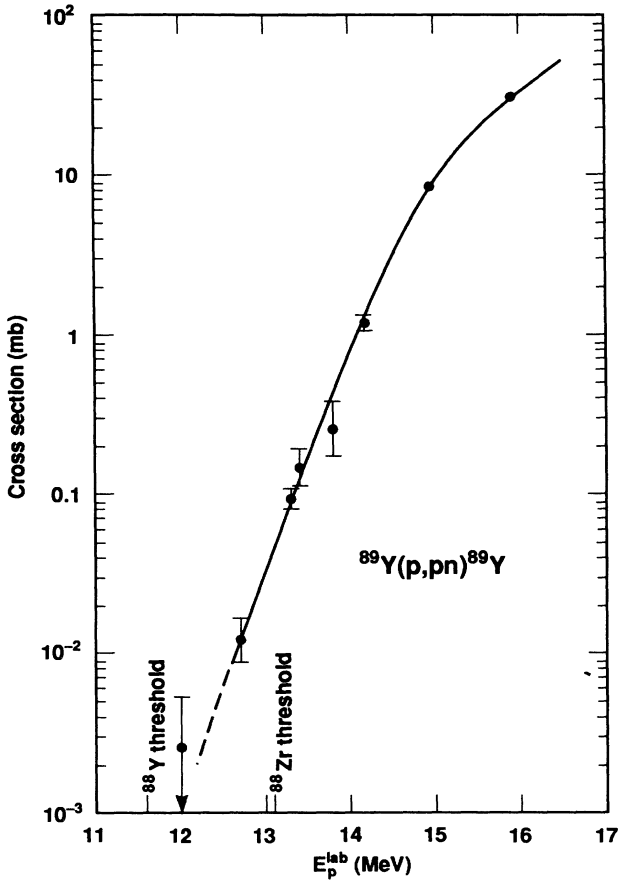

FIG. 8. Low-energy portion of the ^{89}Y$(p,pn)^{88}$Y excitation function.

energy-averaged cross sections for particle-induced reactions as described by the Hauser-Feshbach formalism with angular momentum and parity conservation[5] and width-fluctuation corrections.[20] The HF formalism is well known and HF calculations are routine; however, we shall describe briefly our choice of optical potentials and level densities, the two critical quantities required for a realistic HF calculation.

1. Optical-model potentials

The optical potentials were used to generate particle transmission coefficients or partial absorption cross sections used in the HF calculation. These potentials were chosen from the analysis of experimental data when available and from a sensitivity study of the global potentials otherwise. As is well known, the cross sections in the threshold region are usually very sensitive to the choice of the optical potentials. Fortunately, our choice for the lower energies was guided by the experimental work of Johnson *et al.*[21] for protons below $E_p = 8$ MeV [from a study of ^{89}Y$(p,n)^{89}$Zr data near threshold] and Smith *et al.*[22] for neutrons from $E_n = 1$ to 7 MeV. Below $E_n = 1$ MeV, we used the Moldauer potential.[23] Keeping these lower energy potentials fixed, we then examined the sensitivity of HF cross sections with respect to the proton potentials of Perey,[24] Becchetti and Greenlees,[25] Menet

et al.,[26] and the most recent evaluation by Varner *et al.*[27] For neutrons, we used the potentials of Becchetti and Greenlees,[25] Varner *et al.*,[27] and Rapaport.[28]

The calculated cross sections were not very sensitive to these high-energy neutron potentials; the variation was at most 10%. The cross sections, on the other hand, were fairly sensitive to the choice of the high-energy proton potential. All the proton potentials except for the Perey potential gave similar cross sections. We found as much as 20% difference between the Perey and the other four potentials. This is shown in Fig. 9. It is interesting to note that the Perey potential gave the best fit to the data.

Our final results are, therefore, based on the Johnson potential for $E_p < 8$ MeV and Perey potential for $E_p > 8$ MeV; Moldauer potential for $E_n < 1$ MeV, Smith *et al.* potential for $1 < E_n < 7$ MeV, and Varner *et al.* potential for $E_n > 7$ MeV. Note that alpha particle evaporation is also allowed in our HF calculations, and for that we used the McFadden and Satchler potential.[29]

2. *Level densities*

No experimental data on the continuum level densities are available for the nuclei involved in the HF calculations of the ^{89}Y$(p,xn)^{88,89}$Zr cross sections, i.e., ^{87,88,89,90}Zr, ^{87,88,89}Y, and ^{84,85,86}Sr. We, therefore, had to rely on the systematics of Gilbert and Cameron (constant temperature plus Fermi-gas model)[30] and the back-shifted Fermi-gas model of Dilg *et al.*[31] The parameters of the Gilbert-Cameron level densities were taken from the evaluation of Rose and Cook.[32] The parameters of the back-shifted Fermi-gas model are global: level density parameter $a = A/9$ MeV^{-1}, pairing shift $\Delta = 12/\sqrt{A}$ MeV. For lower energies, we used 25 discrete levels for each nucleus taken from an evaluation of existing data.[33]

It was surprising that the HF cross sections calculated with the back-shifted Fermi-gas model with global parameters gave such an excellent fit to the data (see Fig. 10). We will, therefore, show the remaining calculated cross sections with back-shifted level densities only. Nevertheless, the success of the back-shifted model may not be a global one and it would certainly be interesting to investigate this in other mass regions.

The importance of the discrete levels for the HF calculation is shown in Fig. 11. The effect is as much as 30% (see the region between 15 and 25 MeV).

3. *The gamma-ray strengths*

The gamma-ray strengths are taken from the systematics of Gardner.[34] These were applied successfully to many Hauser-Feshbach calculations.

B. Hauser-Feshbach (HF) plus direct-reaction (DR) cross sections

In the preceding subsection, we discussed the HF calculation and showed that we were able to fit the data rather nicely in the lower E_p regions. Beyond 20 MeV for the (p,n) reaction, however, experiment shows that there is a sizable amount of cross section that cannot be accounted for by the HF theory. Also, a discrepancy between the measured and HF cross sections can be seen for the $(p,2n)$ reaction above 35 MeV [also see Fig. 14 for the (p,pn) reaction]. Here we show that these discrepancies can be reasonably removed by including the direct-reaction (DR) contributions to the reaction mechanism.

The calculation of the DR cross section in the continuum is discussed in detail in Ref. 6. There, the theory is called MSDR theory because the (possible) importance of multistep (MS) contributions is emphasized. In the present application of this theory, however, the maximum neutron energy E_n is given by $E_{\max} = E_p + Q$ ($Q = -3.62$ MeV), and the lowest neutron energy is

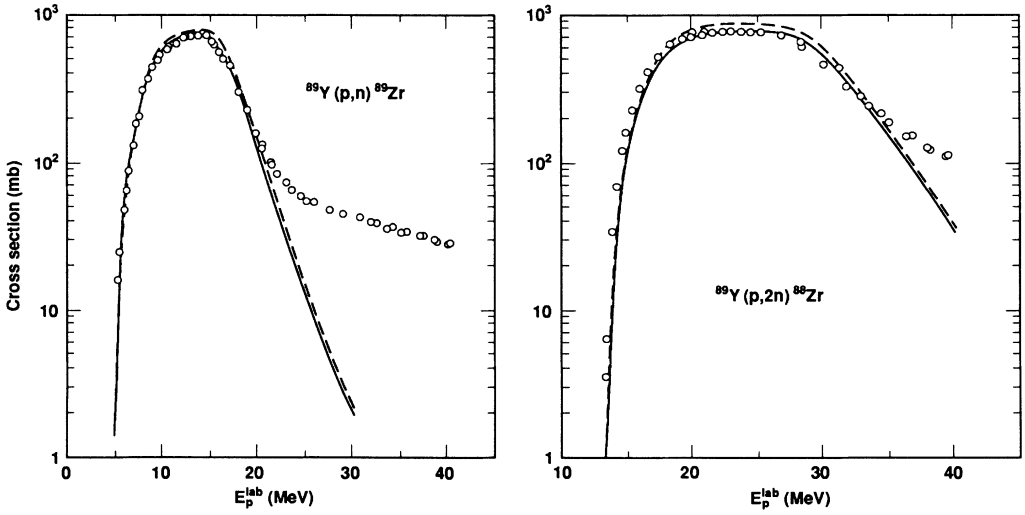

FIG. 9. The sensitivity of the (p,n) and $(p,2n)$ Hauser-Feshbach cross sections with respect to different proton optical potentials above $E_p = 10$ MeV. Results from the Perey (Ref. 24) potential are shown by the solid line and those from the potential of Varner *et al.* (Ref. 27) by the dashed line. The calculations were done using the back-shifted level density parameters: $a = A/9$ and $\Delta = 12/\sqrt{A}$.

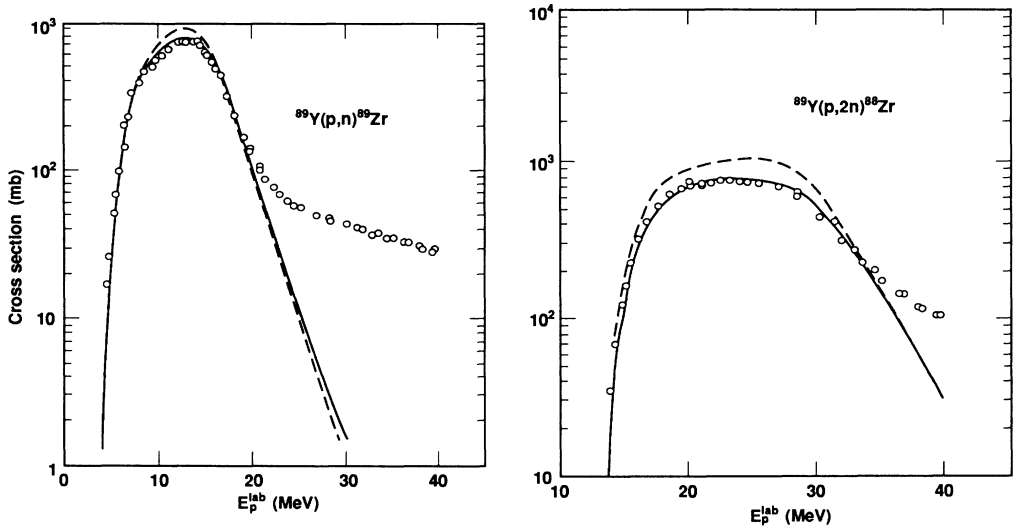

FIG. 10. The sensitivity of the (p,n) and $(p,2n)$ Hauser-Feshbach cross sections with respect to the Gilbert-Cameron (Ref. 32) (dashed line) and back-shifted level density parameters: $a = A/9$ and $\Delta = 12/\sqrt{A}$ (solid line).

given by $E_{\min} = E_{\max} - B_n$, where $B_n = 9.31$ MeV is the neutron binding energy in ^{89}Zr. (If $E_n < E_{\min}$, ^{89}Zr will emit a neutron.) In other words, $E_p - E_n$ and hence the excitation energy of ^{89}Zr must remain rather low; therefore, the contributions of higher step processes should be very small.[6] We show this quantitatively by comparing one- and two-step integrated cross sections in Table II. The one-step cross section (σ_1) is obtained from Eq. (1) (discussed below) integrated over angle θ and neutron energy E_n. The two-step cross section (σ_2) is the sum of $\sigma_{pp'n}$ and $\sigma_{pn'n}$ calculated by the formalism developed in Ref. 6. The cross sections shown in Table II clearly demonstrate that the two-step cross section is indeed very small for the bombarding energies considered in this paper. *We will thus limit our calculation to the one-step process in the present work.*

1. Direct (p,n) cross section

As explained in Ref. 6, we may obtain the continuum (p,n) cross section (double differential), which gives rise to angle-dependent spectra, as

$$\sigma_{pn}(\theta;E_p,E_n) = \sum_l \rho_l(E_p + Q - E_n)\sigma_l(\theta;E_p,E_n) \ . \qquad (1)$$

In Eq. (1), $\rho_l(E_p + Q - E_n)$ is the spectroscopic density and $\sigma_l(\theta;E_p,E_n)$ is the standard DWBA (distorted-wave Born approximation) cross section for the (p,n) process,

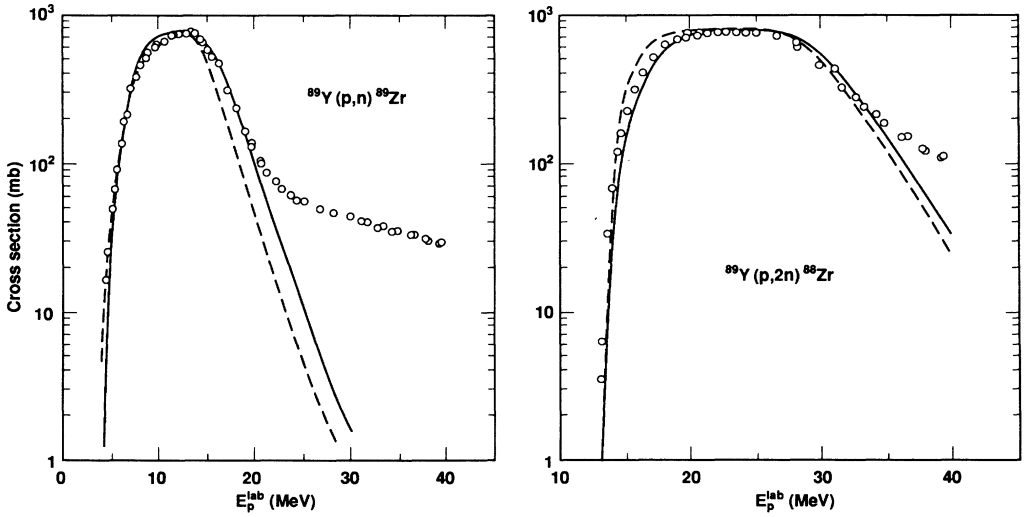

FIG. 11. The effects of the low-energy discrete levels on Hauser-Feshbach cross sections. The solid line shows the results obtained for 25 discrete levels (Ref. 33) and the dashed line shows results without the discrete levels.

TABLE II. One- and two-step direct-reaction cross sections (σ_1 and σ_2) compared with the optical-model total reaction cross section (σ_R) for selected proton bombarding energies for the reaction ^{89}Y$(p,n)^{89}$Zr.

E_p^{lab} (MeV)	σ_R (mb)	σ_1 (mb)	σ_2 (mb)	σ_2/σ_1	$\frac{\sigma_1+\sigma_2}{\sigma_R}$
20	1346	40.0	1.2	0.03	0.03
25	1401	76.1	4.3	0.06	0.06
30	1424	112.5	9.0	0.08	0.09
35	1416	149.1	14.5	0.10	0.12
40	1399	182.1	19.5	0.11	0.14

where l denotes the transferred angular momentum. The DWBA calculation is well known, but we describe in some detail our choice of the form factors. The form factors used are given by[6,7]

$$f_l(r)=\beta_l U(r) \text{ for } (p,n) \text{ reaction},$$
$$f_l(r)=\beta_l R_0(dU/dr) \text{ for } (p,p') \text{ reaction}, \quad (2)$$

where U is the optical potential and R_0 is the radius parameter of the potential. The expressions given by Eq. (2) are normally called the collective form factors. The parameter $\beta_2 \simeq 0.2$ is used, for example, in the analysis of the *collective* 2^+ states in vibrational nuclei (excited through an inelastic scattering process). However, in the present application in which the excitations of a number of noncollective proton-particle and neutron-hole pairs are considered (see below), we find that the use of $\beta_l=0.015$ as a default value for all l is quite appropriate.[6] If this choice is indeed made, $f_l(r)$ is entirely independent of l.

As stated, we consider the direct (p,n) process to proceed as the excitation of particle-hole (ph) pairs, and this consideration is embodied in the construction of the spectroscopic density $\rho_l(E_x)$ that appears in Eq. (1). There, $E_x=E_p+Q-E_n$ is the excitation energy of the residual nucleus, and ρ_l is given as

$$\rho_l(E_x)=\frac{1}{\pi}\sum_{j_p j_h} \text{Im}\left[\frac{|\langle j_p \| i^l Y_l \| j_h\rangle|^2}{E_x-E_{j_p,j_h}-i\Gamma}\right]. \quad (3)$$

This form of $\rho_l(E_x)$ is obtained from the random-phase approximation.[6,7] Here j_p denotes a proton-particle state, and j_h a neutron-hole state. [Only j_p and j_h pairs that satisfy the triangular condition $l=\mathrm{j}_p+\mathrm{j}_h$ contribute to the sum in Eq. (3).] The quantity Y_l refers to the spherical harmonic Y_{lm}, where the magnetic quantum number m is suppressed. Explicit expression for the above reduced matrix element $\langle j_p \| i^l Y_l \| j_h\rangle$ can be found in Ref. 6.

The quantity in the large parentheses in Eq. (3) is called the single-particle response function,[35] and it shows that we are indeed treating the (p,n) process as due to the formation of a proton particle in a shell-model orbit j_p and of a neutron hole in an orbit j_h. The energies of these shell-model orbits may, thus, be taken simply as the Nilsson orbit (with $\beta_2=0$). Then the calculation of the energy E_{j_p,j_h} is trivial. (E_{j_p,j_h} corresponding to the lowest possible j_p and the highest possible j_h is to be taken as zero.) Finally, the appearance of the width Γ in Eq. (3) signifies that we understand that the strength of a given *ph* pair is distributed over the energy range given by Γ. (Lorentzian distribution.) The default value we use for Γ is 4 MeV. This choice is based on the analyses of many (p,p') and (p,n) data by Tamura, Udagawa, and co-workers of the University of Texas. Some of these results were reported in Ref. 6. We did, however, test the sensitivity of our (p,n) cross section with respect to Γ and found that our calculated cross section is not very sensitive to the choice of Γ. For example, an increase (or decrease) of Γ by 25% showed a decrease (or increase) of the integrated (p,n) cross section by at most 6%.

The meaning of $\rho_l(E_x)$ is thus clear. However, with the computer code ORION-TRISTAR (Ref. 7) we use a slightly more complicated expression than Eq. (3) in our calculation of $\sigma_l(\theta;E_p,E_n)$. To mention briefly, this includes some correlation in the ground state and a normalization of the theoretical cross section to the energy-weighted sum-rule limit.[36]

As remarked earlier, $\sigma_{pn}(\theta;E_p,E_n)$ is to be obtained when one wants to fit data of angle-dependent spectra. In fitting the data of Fig. 3, however, we must integrate Eq. (1) over the angle θ and energy E_n. This is done in the following way.

First, we introduce a new cross section defined as

$$\sigma_l(E_p,E_n)=\int \rho_l(E_p+Q-E_n)\sigma_l(\theta;E_p,E_n)d\Omega. \quad (4)$$

It is seen that the integrand on the right-hand side (rhs) of Eq. (4) is just the summand on the rhs of Eq. (1). Thus it is easy to see that $\sigma_l(E_p,E_n)$ is the angle-integrated cross section with which a neutron is emitted with an energy E_n, leaving the residual nucleus an angular momentum denoted by l. Notice that we are ignoring the target and projectile spins. This simplifies the calculation and is expected to be valid for continuum cross sections.[6] The $\sigma_l(E_p,E_n)$ is also interpreted as the cross section with which ^{89}Zr* is formed with an angular momentum l and an excitation energy $E_x=E_p+Q-E_n$. We may take ^{89}Zr*, which is formed with this spin l and the energy E_x, as the starting point of an HF calculation and calculate the survival probability P_l^s for ^{89}Zr, i.e., the probability of ^{89}Zr being left behind after particle evaporation. Thus, the DR contribution to the activation cross section of ^{89}Y$(p,n)^{89}$Zr for the proton energy E_p is given by

$$\sigma_{pn}(E_p)=\sum_l \int_{E_{\min}}^{E_{\max}} \sigma_l(E_p,E_n)P_l^s(E_p+Q-E_n)dE_n \ . \tag{5}$$

The $\sigma_{pn}(E_p)$ thus calculated is plotted in Fig. 12 and identified by DR. The sum of $\sigma_{pn}(E_p)$ with $\sigma_{\rm HF}(E_p)$ (of the previous subsection) is given by the upper line, identified by HFDR. As seen, it fits the data very well over the whole range, showing that a combined use of the HF and DR theories quite adequately explains the data of the ^{89}Y$(p,n)^{89}$Zr reaction.

In these calculations [with ORION-TRISTAR (Ref. 7)], the single-particle energies of the Nilsson model are used with the default values for $\Gamma=4$ MeV and $\beta=0.015$. For the optical-model parameters needed for the DWBA calculation, we used those given recently by Varner *et al.*[27] The calculation was done without any parameter search and gave the excellent results shown in Fig. 12.

In concluding the discussion of the ^{89}Y$(p,n)^{89}$Zr reaction analysis, we want to emphasize that the calculation of the DR continuum cross section with ORION-TRISTAR is not as involved as one might suspect. Note that the Nilsson single-particle levels are built in, and the calculation of the $\sigma_{pn}(\theta;E_p,E_n)$ for a given E_p takes a fraction of a second when using a Cray computer.

2. *Direct (p,2n) cross section*

We now turn to the analysis of the ^{89}Y$(p,2n)^{88}$Zr data. As shown in the preceding subsection, this time the HF cross section accounts for the data to about $E_p\simeq 35$ MeV, and thus the remaining cross section to be explained by DR is seen only in the range of $E_p\simeq 35$–40 MeV. Note that the HF contribution to the $(p,2n)$ cross section $\sigma_{\rm HF}$ is given by

$$\sigma_{\rm HF}(E_p)=\sigma_{\rm HF}^{\rm OM}(E_p)\left[1-\frac{\sigma_R^{\rm DR}(E_p)}{\sigma_R^{\rm OM}(E_p)}\right],$$

where OM refers to the optical model and $\sigma_R^{\rm OM}$ is the optical-model reaction cross section for protons. The direct-reaction cross section $\sigma_R^{\rm DR}$ in principle should include all the direct-reaction cross sections, but in practice, we include only the two dominant processes. These are the direct (p,n) reaction leading to the formation of ^{89}Zr* and the direct (p,p') reaction leading to the formation of ^{89}Y*. The quantity $\sigma_{\rm HF}^{\rm OM}$ is the $(p,2n)$ cross section for HF process only, i.e., $\sigma_R^{\rm DR}=0$. This kind of scaling was unimportant for the (p,n) reaction.

The DR contribution to the production of ^{88}Zr is calculated as

$$\sigma_{p,nn}(E_p)=\sum_l \int_{E_{\min}}^{E_{\max}} \sigma_l(E_p,E_n)P_l^d(E_p+Q-E_n)dE_n \ . \tag{6}$$

This is the cross section to form ^{88}Zr*, by first going through the DR step of the ^{89}Y$(p,n)^{89}$Zr* reaction, followed by a HF emission of a neutron. Thus P_l^d is the one-neutron emission probability from ^{89}Zr*. If the excitation energy in ^{88}Zr* is above the particle emission threshold, of course, the survival probability of ^{88}Zr is calculated as was done for ^{89}Zr [see Eq. (5)]. The survival and decay probabilities are calculated by the STAPRE code. The cross section given in Eq. (6) minus any particle decay is exactly what we referred to above as the DR contribution to the ^{89}Y$(p,2n)^{88}$Zr reaction.

In Fig. 13 we identify the DR contribution to the production of ^{88}Zr by DR, and the sum of HF and DR con-

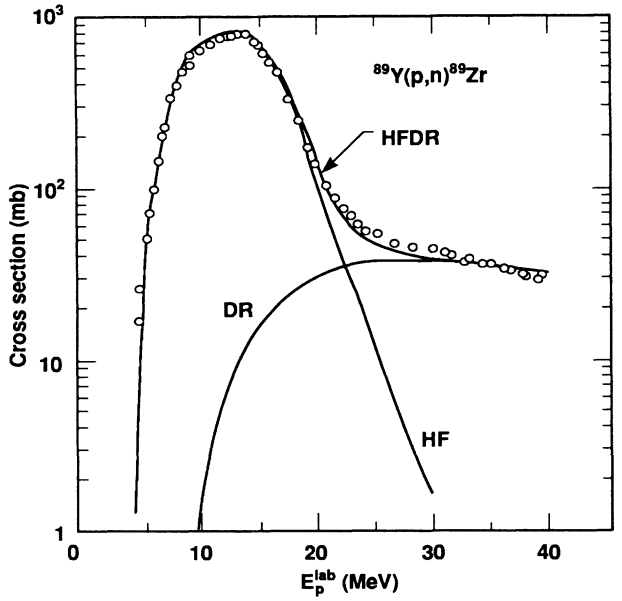

FIG. 12. Hauser-Feshbach (HF), one-step direct reaction (DR), and the total (HFDR) cross sections compared with the present measurements from Table I (circles) for the (p,n) reaction.

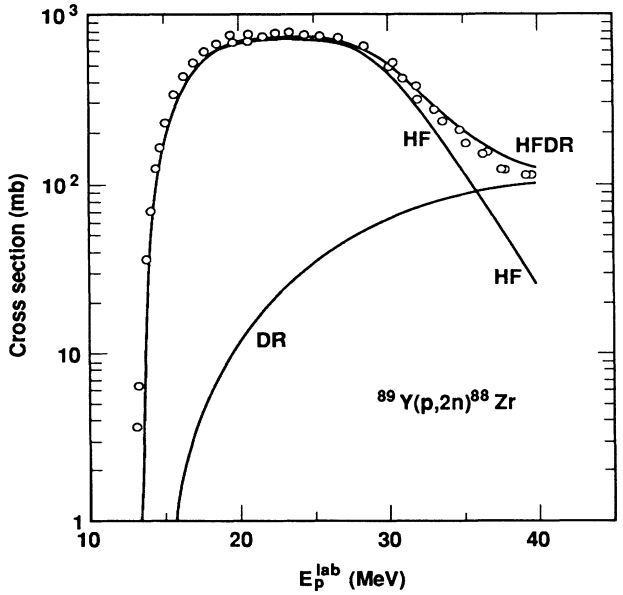

FIG. 13. Hauser-Feshbach (HF), one-step direct reaction (DR), and the total (HFDR) cross sections compared with present measurements from Table I (circles) for the $(p,2n)$ reaction.

tributions by the upper solid line. It is seen that the sum improves the fit to the data, allowing us to conclude that the combination of the HF and DR theories is sufficient to account for the $^{89}Y(p,2n)^{88}Zr$ data as well.

3. The (p,pn) cross section

The results for $^{89}Y(p,pn)^{88}Y$ are shown in Fig. 14. As in the $(p,2n)$ reaction, a large part of the cross section is accounted for by the Hauser-Feshbach evaporation, except for $E_p > 30$ MeV. Also as in the $(p,2n)$ reaction, the HF contribution to the (p,pn) reaction σ_{HF} is obtained from

$$\sigma_{HF}(E_p)=\sigma_{HF}^{OM}(E_p)\left[1-\frac{\sigma_R^{DR}(E_p)}{\sigma_R^{OM}(E_p)}\right],$$

where σ_R^{DR} refers to the sum of the direct (p,n) and (p,p') cross sections and σ_R^{OM} is the usual optical-model reaction cross section for protons. The quantity σ_{HF}^{OM} is the (p,pn) cross section for HF process only, i.e., $\sigma_R^{DR}=0$. The direct-reaction contribution to the (p,pn) activation cross section (identified by DR in the figure) is composed of two parts: (a) the direct (p,n) reaction leading to the formation of $^{89}Zr^*$ and then followed by the HF evaporation of a proton, and (b) the direct (p,p') reaction leading to the formation of $^{89}Y^*$ and then followed by the HF evaporation of a neutron. The sum of these two contributions is then added to the σ_{HF} to obtain the total (p,pn) cross section (upper solid line, identified by HFDR).

Figure 14 shows a fair fit to the data, certainly not as good as for the (p,n) and $(p,2n)$ reactions. However, the importance of the direct reaction above 30 MeV and the dominance of the direct-reaction contribution at 40 MeV are evident.

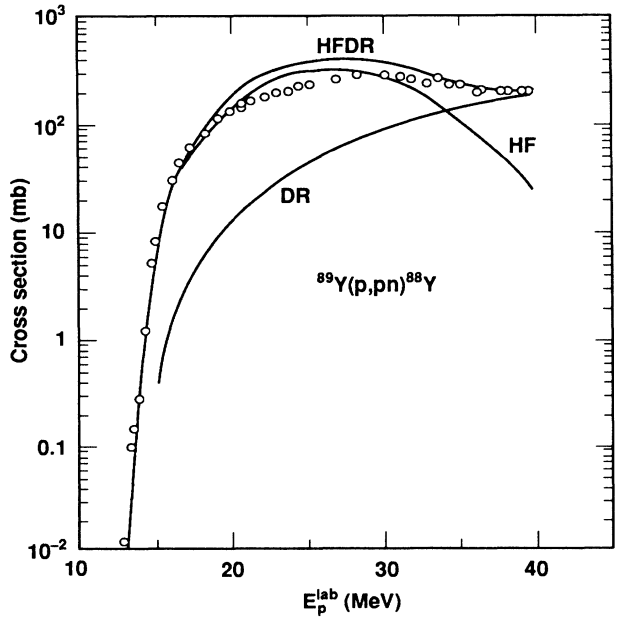

FIG. 14. Hauser-Feshbach (HF), one-step direct reaction (DR), and the total (HFDR) cross sections compared with present measurements from Table I (circles) for the (p,pn) reaction.

We note that the cross section for the (p,pn) reaction near threshold (see Fig. 8) is quite small compared with, for example, the $(p,2n)$ data. Interestingly, we find that the HF calculations show a similar behavior, which suggests that no new physics is present. However, there is enough difference between experiment and the calculation to suggest the need for further examination of the level densities and optical potentials used and the contribution from the direct reactions.

IV. COMPARISON OF SEMICLASSICAL PREEQUILIBRIUM MODEL AND DIRECT-REACTION RESULTS

Since we have already shown that HF + DR theory fits the $^{89}Y(p,n)^{89}Zr$, $^{89}Y(p,2n)^{88}Zr$, and $^{89}Y(p,pn)^{88}Y$ data very well, we could stop our theoretical argument here. Nevertheless, the exciton model[37] has been used extensively to analyze this type of data, and it would therefore seem appropriate to comment on it. For this purpose, we show some results for the (p,n) reaction calculated with the exciton, hybrid, and geometry-dependent hybrid (GDH) models,[38] using global parameters.[39] This work will also test the predictive limits of these preequilibrium models.

The exciton-model calculations were done with the Livermore version of the STAPRE code.[18,19] In this model the exciton transition rates were calculated by the formulas of Williams,[40] corrected for the Pauli principle by Cline.[41] The average residual two-body matrix element that appears in the rate expressions, which determine the transition to equilibrium, was chosen to be

$$|M|^2=KA^{-3}E^{-1},$$

where A is the mass number and E is the excitation energy of the composite system. The quantity K is a constant with the dimension of MeV.[3] The particle-emission rates are calculated from detailed balance considerations and with proton and neutron distinguishability factors.[42]

The parameters of this exciton model are then K, initial particles and holes, and the single-particle level density, $g=(6/\pi^2)a$, where a is the level density parameter. In our present calculation we took 2p-1h as the initial exciton configuration and $g=(6/\pi^2)A/9$. Although we will show results with the value of K taken from the work of the Milano group,[43] which happens to be the default choice for the Livermore version of the STAPRE code, in our opinion K (or g) is a free parameter of the model.

There are, of course, many refinements of the exciton model.[44,45] In our opinion a realistic global set of parameters does not exist, and one usually has to treat at least one parameter as free.

The hybrid and GDH calculations were done with the ALICE code[46] using *all* default parameters,[39] starting with 2p-1h as initial exciton configuration. Also, for convenience, we have used default optical potentials with the ALICE calculations, rather than those described in Sec. III. However, for the present discussion, these differences in the codes and calculations are not important, since in this

subsection we are primarily interested in the high-energy part of the (p,n) cross section.

Figure 15 shows the results for the reaction $^{89}Y(p,n)^{89}Zr$ with global parameter for the exciton model and GDH model. For comparison, we also show the HFDR result, taken from Fig. 12. Note that we took the value of $K=400$ MeV^3 as default in the STAPRE code (as arbitrary choice). This value is suggested by the work of the Milano group[43] and by our limited experience.[1] However, we have done calculations with parameters, $K=405$ MeV^3 and $g=A/13$ MeV^{-1}, and appropriate transition rates as given by Kalbach.[47] The calculations show about 10% lower cross sections than those shown here for the exciton model. In this figure, we only show the default GDH results.

The calculated cross sections shown in Fig. 15 agree with the data to within 50%. However, the agreement can be significantly improved if one varies the parameter K in the exciton model (Fig. 16) and the mean-free path in the hybrid or GDH models (see Fig. 17). Similar agreement can also be achieved by adjusting the parameter g. Note also the successful analysis of the earlier (p,n) data by Birattari *et al.*[13] and Gadioli *et al.*,[48] using the HF and a phenomenological preequilibrium model. These authors have analyzed data for many (p,n) reactions, but a good fit to the data always required an adjustable parameter.

We have not done an extensive analysis of the present data with many refinements of the exciton model. But we believe that the essential physics is included here. An open question, however, is the role of shell effects on the exciton state densities. This may be important since our target-projectile composite is a closed shell. This may be the reason why the global GDH model did not fit the data as well as we would have expected. Some progress in this regard has been reported by Scobel *et al.*[49]

Although our presentation in this section was limited to the (p,n) reaction, the arguments given for this reaction apply also to the $(p,2n)$ and (p,pn) reactions. Our conclusion at this time is that present preequilibrium

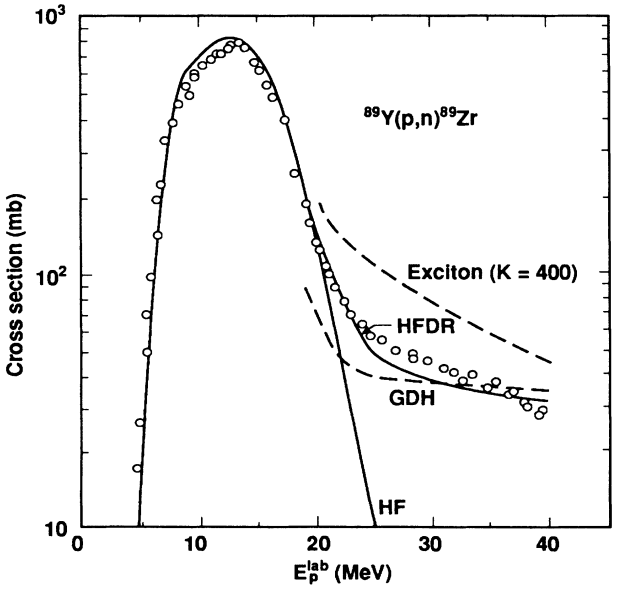

FIG. 15. The analysis of the $^{89}Y(p,n)^{89}Zr$ reaction. The Hauser-Feshbach (HF) plus one-step direct-reaction cross sections (HFDR) are compared with HF plus phenomenological preequilibrium model [exciton and geometry-dependent hybrid (GDH)] calculations with global parameters.

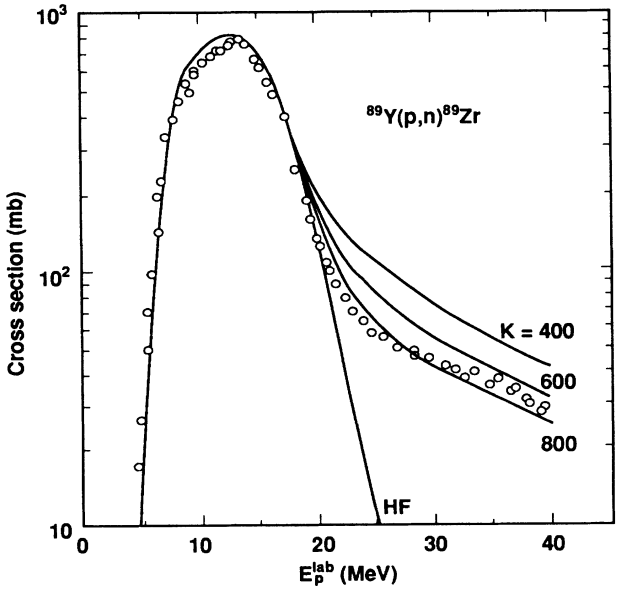

FIG. 16. The analysis of the $^{89}Y(p,n)^{89}Zr$ reaction. The results show the sensitivity of the cross sections with respect to the exciton model parameter K. Notice that a good fit to the data can be obtained.

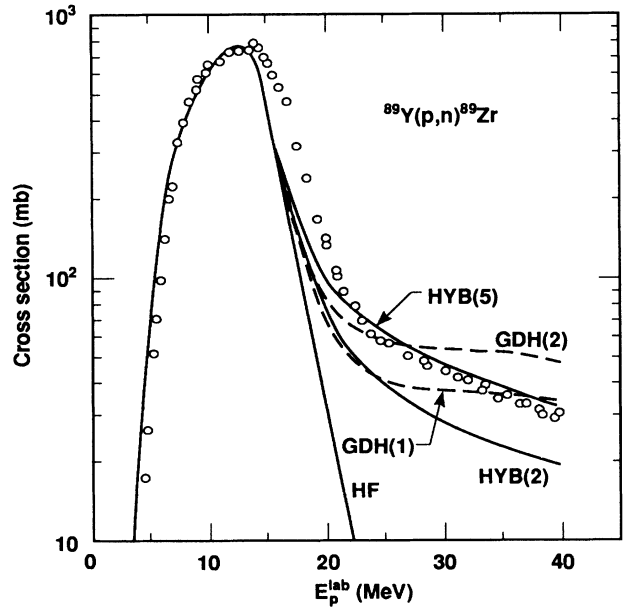

FIG. 17. The analysis of the $^{89}Y(p,n)^{89}Zr$ reaction. The results show the sensitivity of the cross sections with respect to the hybrid (HYB) and geometry-dependent hybrid (GDH) model calculations using the nucleon mean-free path as a free parameter (the numbers in parenthesis are the mean-free-path multipliers). Notice that a good fit to the data can also be obtained by adjusting the mean-free path.

models with global parameters can fit the data to within 50%. Our successful analysis of the data with the microscopic DR theory provides an alternative to these phenomenological models.

V. PHYSICS OF THE DIRECT-REACTION THEORY AND EXCITON MODEL

The physics of our DR theory and that of the exciton model are in fact very closely related. With the exciton model, one starts with thinking of the formation of a three-exciton (2p-1h) state. Once a (high-energy) neutron is emitted, the residual system is of a 1p-1h nature. As explained in Sec. III B, our DR calculation also leaves the residual nucleus ^{89}Zr in 1p-1h states.

In spite of this similarity, however, a significant departure of the two theories begins to take place once the reaction dynamics becomes an issue. As also explained in Sec. III B, our DR theory treats the emission of the neutron [in the (p,n) process] in terms of the DWBA theory, a theory which has been well established. With the exciton model, on the other hand, the emission of a neutron from the 2p-1h is described essentially as an evaporation. (That is, the emission probability is treated as proportional to the absorption cross section from the inverse process.) This evaporation concept is used abundantly in the HF calculation, and its use there may be justified because the HF process is dominated by the emission of rather low-energy nucleons. What is done with the exciton model is to extrapolate the use of the evaporation concept to the emission of rather high-energy nucleons. The validity of this extrapolation may, however, be questionable.

There is another physical aspect involved in the formulation of the exciton model. It is the calculation of the probability with which a 2p-1h state goes into 3p-2h states in competition with the neutron emission. In principle, this probability may be calculated if the cross section of nucleon-nucleon collision inside a nucleus is known. How to calculate this cross section unambiguously is not so well known, however, and this is why the exciton model introduces the parameter K.

With our DR theory, on the other hand, we can easily calculate the cross section for forming a 3p-2h state, or more precisely a state which contains an outgoing high-energy neutron plus the residual nucleus, the latter being left in a 2p-2h state. All we need to do is to extend the one-step DWBA calculation to a two-step calculation in which, for example, the neutron produced in the first-step (p,n) reaction is rescattered by the residual nucleus before it leaves the nuclear field. (How to calculate such two-step cross sections was explained in detail in Ref. 6.) To be emphasized here is the fact that it is totally unnecessary to introduce any new physical concept or any new parameter in extending the calculation from a one-step to two-step process. Our MSDR theory has this appealing feature because it is a microscopic theory.

In summary, our DR theory is very similar to the exciton model regarding the overall physical concept. The two concepts differ, however, rather importantly in dynamics. Our success in fitting a number of data, including those of angle-dependent spectra,[6] convinces us that the dynamics in our model is basically correct. The dynamics behind the exciton model may not be sufficiently appropriate.

As is well known, Feshbach, Kerman, and Koonin (FKK)[50] developed a MSDR-type theory which is closely related to ours.[6] When the application is limited to one step, FKK and our theories are exactly the same. In calculating the higher-order process, however, FKK made a few drastic approximations whose validity may be questioned.[51] In any case, for a set of chosen input parameters, FKK theory generally tends to overestimate the MSDR cross sections compared with ours.

VI. SUMMARY

We have reported the measurement and analysis of cross sections up to 40 MeV for the following reactions: ^{89}Y$(p,n)^{89}$Zr, ^{89}Y$(p,2n)^{88}$Zr, and ^{89}Y$(p,pn)^{88}$Y. The overall accuracy of our measured cross sections is about 3%. Our data have been compared with other measurements and the differences pointed out and discussed.

The cross-section data were analyzed by the Hauser-Feshbach evaporation plus one-step, direct-reaction calculations. We have discussed the range of validity of the one-step direct reaction and provided numerical comparisons of the one- and two-step cross sections. It was shown that the experimental cross sections are well reproduced by the HF plus one-step direct reaction. For completeness, we have also compared some of the data against HF plus phenomenological preequilibrium model calculations and have shown that a good fit to the data can be achieved with these models as well, but requires one free parameter. The calculations with the present global parameters of the preequilibrium models fit the data to within 50%.

In conclusion, we have provided an understanding of the low-energy activation cross sections using a microscopic, quantum mechanical reaction theory, without the need to introduce the phenomenological preequilibrium models.

ACKNOWLEDGMENTS

We thank the operators of the Cyclograaff at the Lawrence Livermore National Laboratory and the operators of the Crocker Nuclear Laboratory Cyclotron, the University of California at Davis, for providing the irradiations. R. Anderson helped with the radiation counting. We acknowledge helpful discussions with M. Blann of the Lawrence Livermore National Laboratory and W. Scobel of Universität Hamburg. This work was performed under the auspices of the U.S. Department of Energy at the Lawrence Livermore National Laboratory under Contract No. W-7405-ENG-48.

*Permanent address: Los Alamos National Laboratory, P.O. Box 1663, Los Alamos, NM 87545.
†Permanent address: Route 1, Box 63T, Dale, TX 78616.
‡Permanent address: Department of Physics, University of Texas, Austin, TX 78212.

[1]H. I. West, Jr., R. G. Lanier, and M. G. Mustafa, Phys. Rev. C **35**, 2067 (1987).
[2]M. G. Mustafa, T. Tamura, and T. Udagawa, Phys. Rev. C **35**, 2077 (1987).
[3]T. Udagawa, B. T. Kim, and T. Tamura, Phys. Rev. C **32**, 124 (1985); B. T. Kim, T. Udagawa, and T. Tamura, *ibid.* **33**, 370 (1986).
[4]T. Udagawa and T. Tamura, Phys. Rev. C **24**, 1248 (1981); **33**, 494 (1986).
[5]W. Hauser and H. Feshbach, Phys. Rev. **87**, 336 (1952).
[6]T. Tamura, T. Udagawa, D. H. Feng, and K. K. Kan, Phys. Lett. **66B**, 109 (1977); T. Tamura, T. Udagawa, and H. Lenske, Phys. Rev. C **26**, 379 (1982).
[7]T. Tamura, T. Udagawa, and M. Benhamou, Comput. Phys. Commun. **29**, 391 (1983).
[8]R. Gunnink and J. B. Niday, Lawrence Livermore National Laboratory Report No. UCRL-51061, 1972 (unpublished).
[9]C. M. Lederer, V. S. Shirley, E. Browne, J. N. Dairiki, R. E. Doebler, A. A. Shihab-Eldin, L. J. Jardine, J. K. Tuli, and A. B. Buyrn, *Table of Isotopes,* 7th ed. (Wiley, New York, 1978).
[10]D. M. Van Patter and S. M. Shafroth, Nucl. Phys. **50**, 113 (1964).
[11]B. P. Bayhurst and G. W. Butler, private communication.
[12]G. B. Saha, N. T. Porile, and L. Yafe, Phys. Rev. **144**, 962 (1966).
[13]C. Birattari, E. Gadioli, E. Gadioli Erba, A. M. Grassi Strini, G. Strini, and G. Tagliaferri, Nucl. Phys. **A201**, 579 (1973).
[14]V. T. Gritsyna, A. P. Klycharev, V. V. Remaev, and L. N. Reschetova, Zh. Eksp. Teor. Fiz. **44**, 1770 (1963) [Sov. Phys.—JETP **17**, 1186 (1963)].
[15]C. H. Johnson, R. L. Kernell, and S. Ramavataram, Nucl. Phys. **A107**, 21 (1968).
[16]J.-P. Blaser, F. Boehm, P. Marmier, and P. Scherrer, Helv. Phys. Acta **24**, 441 (1951).
[17]M. Gusakow, Ph.D. Thesis, Faculte des Sciences de l'Université de Paris, 1962; see also Ref. 10.
[18]D. G. Gardner, private communication.
[19]M. Uhl and B. Ströhmaier, Institut für Radiumforschung und Kernphysik, Vienna, Report No. IRK 76/01 with Addenda, 1976 (unpublished).
[20]P. A. Moldauer, Rev. Mod. Phys. **36**, 1079 (1964).
[21]C. H. Johnson, A. Galonsky, and R. L. Kernell, Phys. Rev. C **20**, 2052 (1979).
[22]A. B. Smith, P. T. Guenther, and J. F. Whalen, Nucl. Phys. **A415**, 1 (1984).
[23]P. A. Moldauer, Nucl. Phys. **47**, 65 (1963).
[24]F. G. Perey, Phys. Rev. **131**, 745 (1963).
[25]F. D. Becchetti, Jr. and G. W. Greenlees, Phys. Rev. **182**, 1190 (1969).
[26]J. J. H. Menet, E. E. Gross, J. J. Malanify, and A. Zucker, Phys. Rev. C **4**, 1114 (1971).
[27]R. L. Varner, T. B. Clegg, T. L. McAbee, and W. J. Thompson, Phys. Lett. **185B**, 6 (1987).
[28]J. Rapaport, Phys. Rep. **87**, 25 (1982).
[29]L. McFadden and G. R. Satchler, Nucl. Phys. **84**, 117 (1966).
[30]A. Gilbert and A. G. W. Cameron, Can. J. Phys. **43**, 1446 (1965).
[31]W. Dilg, W. Schantl, H. Vonach, and M. Uhl, Nucl. Phys. **A217**, 269 (1973).
[32]E. K. Rose and R. L. Cook, Australian Atomic Energy Commission Report No. AAEC/E419, 1977 (unpublished).
[33]E. A. Henry, private communication.
[34]D. G. Gardner, in *Neutron Radiative Capture,* Vol. 3 of *Neutron Physics and Nuclear Data in Science and Technology,* edited by R. E. Chrien (Pergamon, New York, 1984), p. 62.
[35]A. Bohr and B. R. Mottelson, *Nuclear Structure* (Benjamin, London, 1975), Vol. II.
[36]G. R. Satchler, Nucl. Phys. **A195**, 1 (1972); Phys. Rep. **14C**, 97 (1974).
[37]J. J. Griffin, Phys. Rev. Lett. **17**, 478 (1966).
[38]M. Blann, Annu. Rev. Nucl. Sci. **25**, 123 (1975).
[39]M. Blann and H. K. Vonach, Phys. Rev. C **28**, 1475 (1983).
[40]F. C. Williams, Jr., Phys. Lett. **31B**, 184 (1970); Nucl. Phys. **A166**, 231 (1971).
[41]C. K. Cline, Nucl. Phys. **A195**, 353 (1972).
[42]C. K. Cline, Nucl. Phys. **A193**, 417 (1972).
[43]G. M. Braga-Marcazzan, E. Gadioli-Erba, L. Milazzo-Colli, and P. G. Sona, Phys. Rev. C **6**, 1398 (1972).
[44]P. Oblozinský, I. Ribanský, and E. Beták, Nucl. Phys. **A226**, 347 (1974).
[45]C. Kalbach, Phys. Rev. C **33**, 818 (1986).
[46]M. Blann, private communications.
[47]C. Kalbach, Z. Phys. A **287**, 319 (1978).
[48]E. Gadioli, E. Gadioli-Erba, and P. G. Sona, Nucl. Phys. **A217**, 589 (1973).
[49]W. Scobel, M. Blann, T. T. Komoto, M. Trabandt, S. M. Grimes, L. F. Hansen, C. Wong, and B. A. Pohl, Phys. Rev. C **30**, 1480 (1984).
[50]H. Feshbach, A. K. Kerman, and S. Koonin, Ann. Phys. (N.Y.) **125**, 429 (1980).
[51]T. Udagawa, K. S. Low, and T. Tamura, Phys. Rev. C **28**, 1033 (1983).